Annals of Nuclear Energy 125 (2019) 138–147

Contents lists available at ScienceDirect

Annals of Nuclear Energy

journal homepage: www.elsevier.com/locate/anucene

Evaluation of activated corrosion products in primary coolant circuit of AP-1000 under grid frequency stability mode

Fiaz Mahmood, Huasi Hu *, Liangzhi Cao, Guichi Lu, Si Ni, Jiaqi Yuan

School of Nuclear Science and Technology, Xi'an Jiaotong University, Xi'an, Shaanxi 710049, China

ARTICLE INFO

Article history:
Received 3 July 2018
Received in revised form 7 September 2018
Accepted 16 October 2018
Available online 30 October 2018

Keywords:
Activated corrosion products
Specific activity
Primary coolant circuit
Power transients
CPA-AP1000

ABSTRACT

The AP1000 is a strong candidate to participate in grid frequency stability because of its better transient response capability. The investigations are essential to sort the behavior of activated corrosion products (ACPs) under frequency control induced power transients. This paper seeks to assess the variation of ACPs in the primary coolant circuit of AP-1000 under base-load as well as grid frequency stability modes. The computer program CPA-AP1000 is modified to incorporate frequent power fluctuations. The simulation results depicted that short-lived ACPs (^{56}Mn, ^{24}Na) build up fairly rapidly whereas long-lived ^{59}Fe, ^{99}Mo, ^{58}Co and ^{60}Co exhibited slow rise, under customized base-load mode. All of the ACPs are noticed to attain a saturation value of specific activity after several hours of the reactor operation. The corresponding ACPs (^{56}Mn, ^{24}Na, ^{59}Fe, ^{58}Co, ^{99}Mo and ^{60}Co) in the primary coolant under frequency fluctuation mode, are noted to be governed by the rise and fall in operating power level. The investigations are extended to compare the variation in the behavior of ^{56}Mn, ^{24}Na, ^{58}Co, and ^{60}Co in primary coolant and on the inner walls of piping and core structure, under the grid frequency stability mode. The activity due to corresponding ACPs is the highest inside the core followed by the coolant and piping structure. The results revealed that activity associated with ACPs with shorter half-lives is more susceptible to power oscillations, as compared to those having longer half-lives. The post-fluctuation activity of corresponding ACPs is also explored and found to be significantly dependent on the final and post-fluctuated power levels. The long-term dose of ACPs with longer half-lives is found to be more significant, because their activity holds for an extended spell. This study provides a good insight into on-power accessibility of the primary coolant circuit for recurrently happening operating scenarios.

1. Introduction

The corrosion of the metals in contact with water is inevitable and generates the corrosion products (CPs), which are neutron activated while passing through the reactor core. These activated corrosion products (ACPs) emit harmful gamma-rays contributing almost 90% of occupational radiation exposure (ORE) during operation and maintenance activities at PWRs (Zhang et al., 2016). The half-lives of ACPs are >2 h, which specifies that primary coolant will keep activity even after several hours of the reactor shutdown (Nasir et al., 2017). The half-lives of major ACPS are shown in Table 1. The operational and post-shutdown activities are seriously affected due to a huge amount of ORE caused by the ACPs. These radiation levels are two orders higher magnitude for PWR systems as compared to gas or sodium cooled reactors. Consequently, operation and maintenance activities are prolonged, resulting in an increased reactor downtime and substantial revenue loss of several million dollars per annum (Rafique et al., 2010). The response of ACPs in the primary coolant circuit is strongly dependent on the reactor operating parameters. These parameters include interacting materials composition, coolant impurities, operating power, coolant residence time in the core and rest of the circuit, temperature, pressure, coolant flow rates, corrosion rates, filter efficiency and ACPs deposition rates (Malik et al., 2012). The longer cycle length and flexible operating strategies of modern reactor designs can also induce complicated effects on the buildup and decay behavior of ACPs.

Currently, large and multiple grid systems are being used to fulfill the growing energy demands of the world. These systems are at high risk of power imbalances because of contributions from the intermittent power supply sources. The NNPs have been mostly used for base-load operation with few exceptions in the world. However, the fresh NPPs are made mandatory to be capable of complying with grid frequency transients, because of the growing contribution from NPPs in many national grids (Ponciroli et al.,

* Corresponding author.
E-mail address: huasi_hu@mail.xjtu.edu.cn (H. Hu).

https://doi.org/10.1016/j.anucene.2018.10.031
0306-4549/

Table 1
Corrosion products and their reaction properties (Nasir et al., 2017).

Sr. #	Reaction	Corrosion product	Activation cross section	γ-ray energy
1	^{23}Na (n, γ) ^{24}Na (E_n > 11.60 MeV)	^{24}Na ($T_{1/2}$ = 15.40 h)	0.530b	4.10 MeV
2	^{58} Fe (n, γ) ^{59}Fe (E_n is thermal)	^{59}Fe ($T_{1/2}$ = 45.10 h)	0.900b	1.17 MeV (99.99%) 1.33 MeV (99.99%)
3	^{98}Mo (n, γ) ^{99}Mo (E_n > 3.10 MeV)	^{99}Mo ($T_{1/2}$ = 67.00 h)	0.450b	0.78 MeV (8%) 0.74 MeV (8%)
4	^{59}Co (n, γ) ^{60}Co	^{60}Co ($T_{1/2}$ = 5.30 y)	20.000b	1.17 MeV (99.99%) 1.33 MeV (99.99%)
5	^{55}Mn (n, γ) ^{56}Mn (E_n is thermal)	^{56}Mn ($T_{1/2}$ = 2.58 h)	13.400b	2.13 MeV (15%) 1.81 MeV (24%) 0.85 MeV (99%)
6	^{59}Ni (n, p) ^{58}Co (E_n is fast)	^{58}Co ($T_{1/2}$ = 70.88 d)	0.146b	

2015). The operating modes are highly evolved and new PWRs are capable of inducing large and rapid power fluctuations during reactor operation (NEA, 2011). The first AP1000 in Zhejiang province of China is seemed to substantially contribute to the local power grids in the near future (World Nuclear News, 2018). China poses serious concerns for the participation of NPPs in stabilizing frequency fluctuations because of already faced grid frequency instability incidents and rapidly increasing nuclear power capacity (Tang et al., 2014). The studies have demonstrated that AP-1000 possess good control capabilities throughout the cycle, with sufficient safety and economy features (Wang et al., 2018). The AP-1000 has enhanced favorability to participate in grid frequency control because of its advantageous Mechanical SHIM (MSHIM) control strategy. This feature provides reactivity control with the control rods movement only in contrast to existing PWRs which are using soluble boron concentration (Westinghouse, 2005). But, the capability of AP-1000 to adopt the demand of participation in grid frequency control has provoked the frequent variation in specific activity of the ACPs in the primary coolant circuit. These variations in the specific activity of ACPs during design-based grid fluctuations are not too large in value but these are rapid and frequent. The study of ACPs behavior during such transients is crucial for the assessment of ORE during on-power accessibility of primary circuit.

The researchers have widely focused to analyze the behavior of ACPs in typical PWRs during last few decades. The behavior of ACPs in typical PWRs is studied in detail by developing computer program CPAIR-P (Deeba et al., 1999; Mirza et al., 1998). The program was later on updated to incorporate the changes in ACPs induced by the linearly and non-linearly increasing corrosion (Mirza et al., 2003). The code was further improved to study coupled effect of time-dependent corrosion and coolant chemistry for long-term fuel cycles (Malik et al., 2012; Nasir et al., 2017). The mitigation of the crud in PWR systems has also been attributed a research emphasis. Shim et al. have recently tested aluminum oxide (Al_2O_3) as a fuel cladding coating to investigate its crud mitigation effects (Shim et al., 2018). The experimental results revealed that crud deposits were decreased by 23% for the Al_2O_3-coated cladding, as compared to the uncoated cladding. Owing to a wealth of operating experience and research efforts, sufficient capability has been established to study ACPs behavior in PWRs. However, the study of CPA in fresh reactor designs is a standing challenge (IAEA, 2012). The research efforts are being put to face this challenge to analyze the ACPs behavior in fresh reactor designs. The operational experience of PWRs has been helpful to envisage the associated problems in new designs of nuclear reactor fleet. The experience has shown that use of a simulation tool, in addition to loop experiments and the plant measurement campaigns, is also crucial in envisaging the contamination by ACPs in the PWR circuits (Benfarah et al., 2016). It can be helpful in the improvement of reactor operating parameters as well as the optimization for the future plant designs.

The study of ACPs behavior in AP-1000 has previously attributed a limited focus mainly because of its fresh design. However, the related research is recently getting more attention from the researchers. The researchers have developed and applied homogeneous and two-node models to calculate activity from the activation products ^{16}N, ^{17}N, ^{3}H and ^{14}C in chosen regions of the AP-1000 primary circuit (Guo et al., 2018). The analyses were extended to assess the respective dose impact, employing the point kernel code ARShield. An in-house computer code CAT 1.0 was developed to visualize the corrosion of structural material and the inhabitation effects induced by the injection of Zn in the primary circuit of AP-1000 (Jia, 2016; Mo Shuran, 2016). The code uses the mixed conduction model to provide a good insight of time-dependent behavior of CPs migration process. However, the activation process and behavior of ACPs under various operating scenarios needs more research. So, the computer program namely Corrosion Products Activity in AP-1000 (CPA-AP1000) was developed to analyze the behavior of ACPs in AP-1000 (Mahmood et al., 2018). The CPA-AP1000 was previously employed to analyze the CPA behavior in the primary coolant of AP-1000 under normal operation and MSHIM based power transients. The aforementioned works do not address the variation of ACPs in different parts of the primary coolant system under frequency control mode. The present study explores the behavior of ACPs in the primary coolant system of AP-1000 under frequency regulations, which are desirable to adapt the grid demands. The behavior of ACPs in different sections of the primary circuit like coolant and inner walls of structures inside the core and piping located outside the core is explored. The simulation methodology as developed in the code CPA-AP1000 is updated to study the behavior of ACPs in the course of frequency regulation.

This paper is structured as follows. Section 2 presents the formulation of the mathematical model along with the assumptions considered for modeling. Section 3 contains the core configuration and necessary parameters of AP-1000. Section 4 comprises the hierarchy of computational scheme. Section 5 presents the simulation results and discussion of the related technical aspects. Section 6 concludes this work and future recommendations are outlined.

2. Mathematical model

The mathematical model is built up by dividing the primary circuit into different zones like reactor core, primary coolant and piping structure outside of the core. The exchange processes in different zones e.g. activation of CPs due to continuous circulation of coolant, deposition, dissolution, erosion, filtration, the decay of the CPs during circulation in the circuit are considered. Different exchange pathways used for modeling are schematically described in Fig. 1. The mathematical model of the time-dependent behavior of dominant CPs in the primary coolant circuit of AP-1000 is established considering the following assumptions (Deeba et al., 1999; Mahmood et al., 2018).

- The composition of CPs corresponds to the chemical composition of original corroding material.
- The material on the walls of the cooling system corrodes uniformly and homogeneously.
- The intrinsic activity is considered to be negligible.
- The deposition on surfaces in contact with cooling water is proportional to the concentration of CPs in water.
- The ion exchangers and filters eliminate impurities corresponding to their concentration in the coolant.

The neutron flux is treated as representative of reactor operating power. The change in neutron flux rate is modeled as directly affected by variation in reactor operating power. In order to incorporate the effect of power maneuvering, the power levels are modeled with the subsequent scheme. The time-dependent operating power$p(t)$ is defined in terms of normalized power parameter $f(t)$ and rated thermal power (RTP) p_0 as following;

$$p(t) = f(t)p_0 \tag{1}$$

The parameter $f(t)$is capable of describing reactor operation at specified power levels as induced by either normal operation or MSHIM based power transients. The power parameter $f(t)$ describes any linear increase or decrease in reactor operational power as following;

$$f(t) = \begin{cases} p_{1,} & t < t_{ts} \\ p_1 - \mu(t - t_{ts}), & t_{ts} \le t < t_{te} \\ p_2, & t \ge t_{te} \end{cases} \tag{2}$$

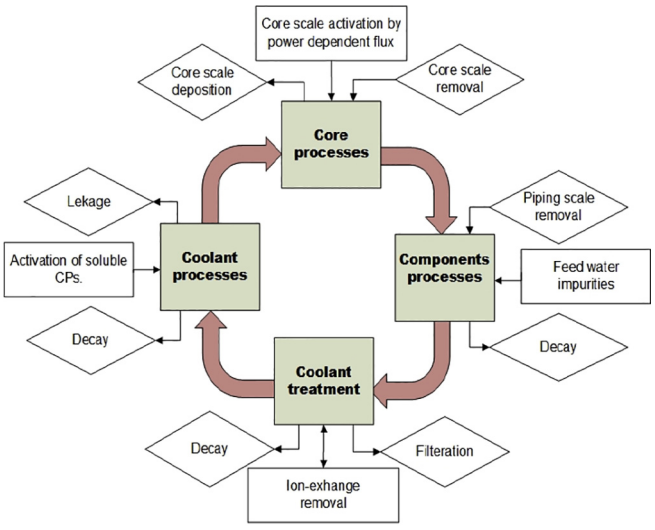

Fig. 1. Schematic of exchange pathways for modeling activation products in the primary coolant circuit.

where p_1 and p_2 represent operating power in terms of percentage *RTP* before start and end of power maneuvering at time $t_{ts}$and t_{te} respectively, and μ is the slope of linear increase or decrease operating power.

The activation of corrosion products is affected by the time taken by a particle for traversing through the primary coolant circuit, and length of time it is exposed to the neutron flux. The effective neutron flux density ϕ_ϵ (n cm^{-2} s^{-1}) links both of these time intervals as following;

$$\phi_\epsilon = \frac{1 - e^{-\lambda T_c}}{1 - e^{-\lambda T_L}}\phi_0 \tag{3}$$

The concentration of target nuclides (atoms cm^{-3}) in the primary coolant, on piping and core surfaces, have been denoted byN_w,N_p and$N_c$respectively. The concentrations of activated nuclides (atoms cm^{-3}) in the primary coolant water, on the inner walls of piping and core surfaces, have been denoted byn_w,n_p, and n_c respectively. The rate of change of active material concentration in primary coolant is given by;

$$\frac{dn_w}{dt} = \sigma f(t)\phi_\epsilon N_w - \left(\sum_j \frac{\varepsilon_j Q_j}{V_w} + \sum_k \frac{l_k}{V_w} + \lambda\right) n_w + \frac{k_p}{V_w} n_p + \frac{k_c}{V_w} n_c \tag{4}$$

where σ is the group constant for the production of the isotope from target nuclide.

The sum over j for $\varepsilon_j Q_j$ is given as following;

$$\varepsilon_j Q_j = \varepsilon_i Q_i + \varepsilon_f Q_f + \varepsilon_c Q_c + \varepsilon_p Q_p \tag{5}$$

where the quantities $\varepsilon_i Q_i, \varepsilon_f Q_f, \varepsilon_c Q_c, \varepsilon_p Q_p$ are removal rates (cm^3 s^{-1}) induced by ion exchanger, filter, core and pipe surfaces respectively. The term l_k is rate (cm^3 s^{-1}) at which the primary coolant is lost during the kth leak, k_p and k_c are rates (cm^3 s^{-1}) at which isotopes are removed from the scale on piping and core respectively. The first term in equation (4) represents the production of radioactive isotopes. The second term is loss rate of active nuclides caused by purification by the ion-exchanger and filter, deposition on the piping and core, and radioactive decay. Third and fourth terms are the rates at which activity is re-introduced into the water as a result of erosion or dissolution of activity deposited on inner surfaces of piping and reactor core. The rate of change in target nuclide concentration in coolant water can be written as;

$$\frac{dN_w}{dt} = -\left(\sum_j \frac{\varepsilon_j Q_j}{V_w} + \sum_k \frac{l_k}{V_w} + \sigma f(t)\phi_\epsilon\right) N_w + \frac{k_p}{V_w} N_p + \frac{k_c}{V_w} N_c + S_w \tag{6}$$

$$S_w = \frac{C_0 S N_0 f_n f_s}{V_w A} \tag{7}$$

where C_0 is effective corrosion rate (g cm^{-2} s^{-1}), S is area of the system exposed to the coolant for corrosion (cm^2), N_0 is Avogadro's number (6.02 x 10^{23} atoms g$^{-1\ mol-1}$), A is atomic weight of target nuclide (g mole^{-1}), f_n is natural abundance of target nuclide and f_s is abundance of target nuclide in the system. The rate of change of active nuclides on the surface of the cooling system inside the reactor core is given by;

$$\frac{dn_c}{dt} = \sigma f(t)\phi_0 N_c + \frac{\varepsilon_c Q_c}{V_c} n_w - \left(\frac{k_c}{V_c} + \lambda\right) n_c \tag{8}$$

The rate of change in target nuclei of the core scale is given by the following balance;

$$\frac{dN_c}{dt} = \frac{\varepsilon_c Q_c}{V_c} N_w - \left(\frac{k_c}{V_c} + \sigma f(t)\phi_0\right) N_c \tag{9}$$

where $V_c$is voluthe me of deposits within the core (cm^3). The rate of change in active material on the piping surface can be obtained from the following relation;

$$\frac{dn_p}{dt} = \frac{\varepsilon_p Q_p}{V_p} n_w - \left(\frac{k_p}{V_p} + \lambda\right) n_p \tag{10}$$

where V_p is the volume of scale on the piping (cm^3).

The rate at which target nuclei change on the piping scale is given by the following relation;

$$\frac{dN_p}{dt} = \frac{\varepsilon_p Q_p}{V_p} N_w - \frac{k_p}{V_p} N_p \tag{11}$$

The above system of coupled differential equations (1–11) is adequate to describe the dynamic response of ACPs under normal operating conditions and a variety of power maneuverings. The system of equations developed in the model is applicable regardless of corrosion pattern. However, a uniform corrosion is considered in the current investigations and space distribution effects are ignored.

3. Core configuration and flux calculations

The AP-1000 is Westinghouse reactor design having rated core power of 3400 MW_{th}. It consumes enriched UO_2 as fuel and light water as a coolant and moderator. The reactor core comprises a matrix of fuel rods lump together into mechanically identical 157 fuel assemblies in conjunction with control and structural elements. The core is proposed for an 18-month fuel cycle having 93% capacity factor and region average discharge burnup of 60,000 MWd/tU. The fuel assemblies are arranged in three radial regions the form of a right circular cylinder having. The core regions are structured in different enrichments to create a favorable power distribution. The fuel enrichment ranges from 2.35% to 4.50% in the first core. The core is covered by light water and stainless steel reflectors at top and bottom, and also in the radial direction. The thickness of the top, bottom, and radial reflector material are nearly 25 cm, 25 cm and 38 cm, respectively. Each fuel assembly of the AP-1000 contains a 17 × 17 square lattice array, in which 264 fuel rods, 24 control rod guide tubes, and one central instrumentation tube are adjusted. The Discrete Burnable Absorbers (PYREX) and Integrated Fuel Burnable Absorber (IFBA) rods are responsible to control the excess reactivity in the initial core. The PYREX rods are supposed to detach from the core at the end of the first cycle. The burnable absorber is introduced for the control of peaking factors. It also regulates the moderator temperature coefficient of the core to avoid its value positive during normal operation. The AP-1000 reactor core contains total nine dissimilar assembly types which are formed by the organization of PYREX and IFBA rods in three and five distinct patterns respectively. The radial enrichment map of the reactor core and fuel assembly configuration of AP-1000 are shown in Fig. 2.

4. Primary coolant system configuration

The primary coolant system, also called the Reactor Coolant System (RCS), consists of the reactor vessel (RV), the steam generators (SGs), the reactor coolant pumps (RCPs), a pressurizer, and the connecting piping. The primary function of the RCS is to transfer the heat from the fuel to the SGs and its second function is to contain the radioactivity within the primary circuit. The AP-1000 has a two-loop RCS, each loop contains a SG and two RCPs (Westinghouse, 2005). It has a single hot leg and two cold legs for circulation of the reactor coolant. Additionally, the system includes the pressurizer, interconnecting piping, valves, and instrumentation for operational control and safeguards actuation. All RCS equipment is located in the reactor containment. A layout diagram of the primary circuit with steam generators is shown in Fig. 3. The RCPs circulate the primary coolant through the RV and the SGs during the reactor operation. The water is heated as it passes through the core. It is then transported to the SGs where the heat is transferred to the steam system. The coolant is ultimately returned to the reactor vessel by the pumps to repeat the process. The RCS pressure is controlled by operation of the pressurizer, where water and steam are maintained in equilibrium by the activation of either electrical heaters or water spray, or both

The RCS pressure boundary is responsible for a barrier against the release of radioactivity and it is for a high degree of integrity throughout operation of the plant. An important characteristic of the RCS is the materials which are in contact with the primary coolant. These particular materials interact with the coolant and therefore govern the vulnerability to corrosion and ultimately the production of ACPs. The AP1000 follows the well-established and industrialized approach of confining the material in contact with the primary coolant. The materials of the parts of RCS interacting with the water are fabricated from or clad with corrosion-resistant materials. The materials exposed to the primary coolant

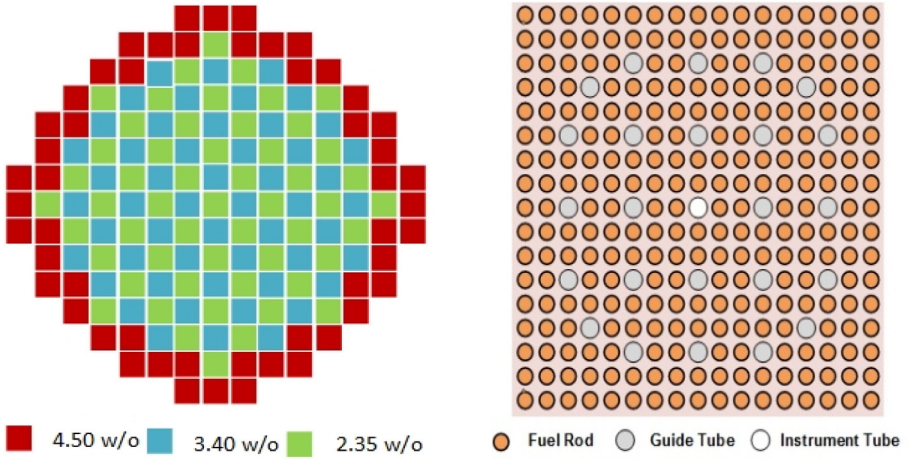

Fig. 2. The radial enrichment map of the reactor core and fuel assembly configuration for AP-1000.

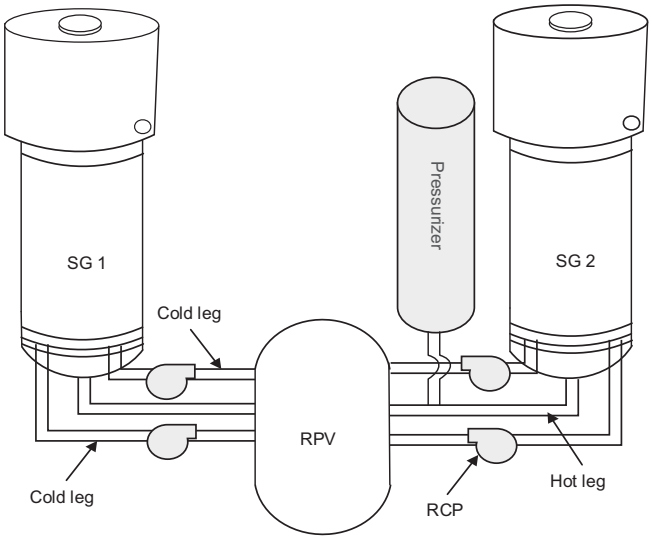

Fig. 3. The layout of the primary circuit with steam generators.

are confined to stainless steels, nickel-chromium-iron alloys, and, to a limited extent, cobalt-based alloys. An important design choice, for the AP1000 RCS is the use of Inconel 690 in the thermally treated state (I690 TT) for the tube material in the SGs. The typical design specifications of the AP-1000 reactor are described in Table 2.

5. Computing scheme

Based on the above model, a computer program namely Corrosion Products Activity in AP-1000 (CPA-AP1000), has been developed by programming in MATLAB. The CPA-AP1000 contains two loops; one loop calculates specific activity under steady-state or power maneuvering conditions, and other moves over different isotopes. After initialization, the program calculates group fluxes using Tally-4 of the MCNP code. Since the MCNP results are normalized to one source neutron, the result has to be properly scaled in order to get the absolute comparison to the measured quantities of flux. Therefore, the scaling factor is applied in data processing and F4 tally results of core averaged group fluxes are scaled to desired fission neutron source (power) level using Eq. (12) (Snoj and Ravnik, 2006).

$$\phi_0 = \frac{P(Watt)\,\bar{\nu}\left(\frac{n}{fission}\right)}{1.6023.10^{-13}\left(\frac{J}{MeV}\right)w_f(MeV/fission)}\phi_{F4} \tag{12}$$

where P is power, $\bar{\nu}$is avthe erage number of neutrons released by fission, w_f is the energy released per fission and ϕ_{F4} is the flux result given by the tally F4. The system of coupled differential equations is solved using 4th order Runge Kutta (RK-4) method. The overall computational scheme is shown in Fig. 4.

6. Results and discussions

The execution of simulations was started at time t = 0, considering the reactor to be operated in the steady state and having no impurities at the early stage. It has been assumed that the system material corrodes uniformly and homogeneously with constant corrosion rate. The primary coolant having a volume of 1.37×10^7 cm^3, is exposed for corrosion of plant surface area of about 1.01×10^8 cm^2 and an equilibrium corrosion rate of 2.4×10^{-13} g. cm^{-2}. s^{-1} is established after reactor operation of one year (Mirza et al., 2003). The conservative value of normal equilibrium corrosion rate of 25 μg. s^{-1} has been selected for the subsequent investigations. The deposition and resolution values for the core and the piping structure are based on loop experiments, in which exchange processes along with reasonable assumptions described in Section 2 are considered. The experimental values of various factional exchange rates for deposition and resolution for the core and the piping structure, used in the current study are shown in Table 3.

The study of the dominant effect of key parameters of the subjected model has identified that ion- exchanger removal is the most sensitive parameter to effect CPA values (Mirza et al., 2010). An approach adopted in our previous study was employed to visualize the detailed effect of ion exchange removal on saturation specific activity of ^{24}Na (Mahmood et al., 2018). The specific

Table 2
Typical design specifications of the AP-1000 reactor (Stefani et al., 2015; Westinghouse, 2005).

Parameter	Design value	Parameter	Design value
Power		Mass of UO_2/m (Kg/m)	6.54
Thermal (MW)	3400	Loops	
Electrical (net) (MW)	1090	Number of cold legs	4
Specific power (kW/kg U)	40.20	Number of hot legs	2
Power density ($MW/m^{3)}$	109.70	Hot leg ID, cm	78.74
Core		Cold leg ID, cm	55.88
Height (m)	4.27	RCP	
Diameter (m)	3.04	Number of RCPs	4
Fuel		Type	Sealless
No. of fuel assemblies	157	Effective pump power, MWt	15
Rod array dimension	17x17	Pressurizer	
Rods per assembly	264	Number of units	1
Rod pitch (mm)	12.60	Height, cm	1277.62
Clad thickness (mm)	0.5715	Inside diameter, cm	254
Fuel loading, UO_2 (kg)	95,974	SG	
Material	UO_2	No. of units	2
Pellet diameter (mm)	8.1915	SG power, MWt/unit	1707.5
Number of fuel rods	41,448	Type	Vertical U-tube
Rod, OD (mm)	9.50	Material	I690 TT
Diameter gap (mm)	0.1651	Coolant	
Dimension of FA (mm x mm)	214 x 214	Pressure (MPa)	15.51
Clad material	ZIRLO	Inlet temperature (°C)	279.44
Fuel pellet length (mm)	9.83	Avg. temperature in core (°C)	303.39
Enrichment levels	2.35w/o, 3.40w/o, 4.50w/o	Total thermal design flow rate of vessel (kg/s)	14300.76

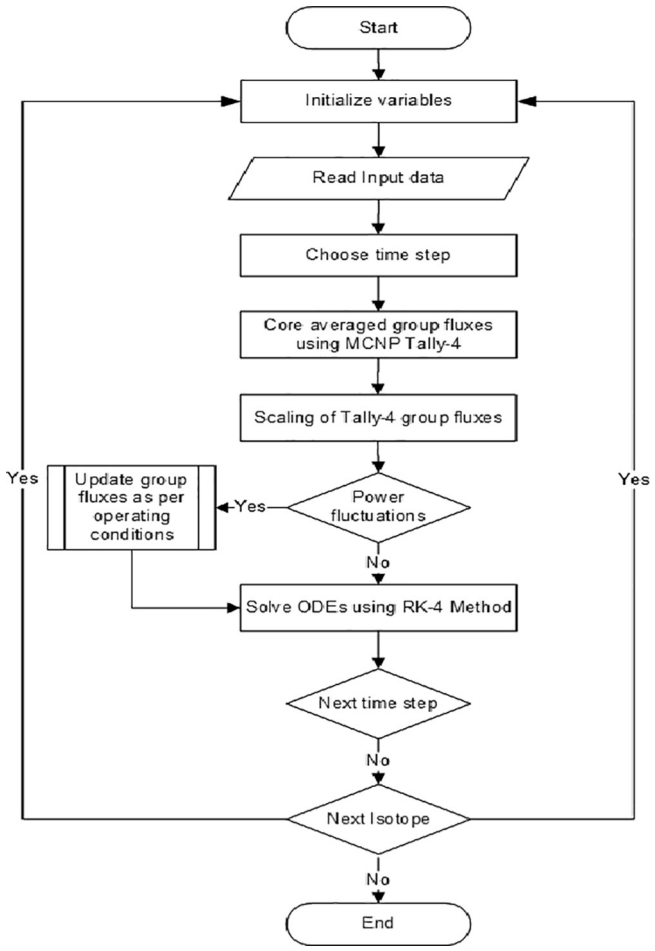

Fig. 4. Flowchart of CPA-AP100 for computing ACPs under various operating modes.

activity of ^{24}Na was calculated for several values of the ion-exchanger removal rate, during reactor operation in steady-state for a particular time. The results depict that saturation activity is higher enough for low ion exchanger removal rate and it drops in a non-linear manner as ion exchanger removal rate is increased. When value of $\varepsilon_I Q_I$ approaches 400 cm^3 s^{-1}, saturation activity fluctuates with a negligible slope and becomes nearly constant at 600 cm^3 s^{-1}. Therefore, the optimum value of ion exchange removal rate of 600 cm^3 s^{-1} was selected for subsequent evaluations.

6.1. The behavior of ACPs under various operating modes

The grid load fluctuates subjected to the varying power demands, and ultimately causes grid frequency fluctuations (NEA, 2011). The power plant participating in frequency stability has to monitor the grid frequency and instantly adjust its operating power level to maintain the desired value of the grid frequency. The operation of NPPs for grid frequency control is characterized by rapid and approximately random oscillations in reactor power level. In this mode of the operation, the reactor can experience frequent power swings up to 10% RTP at ramp power rate fluctuations as large as 5% per minute (Drudy et al., 2009). The MSHIM control strategy is advantageous to control rapid power fluctuations during reactor operation because of automatic reactor control with control rod movements only. This control strategy without inducing variation in soluble boron concentration has an additional benefit of stable axial power distribution control. The behavior of ACPs under various operating modes was studied by allocating distinct operating modes in three specific segments of reactor operation time period as following;

i. Customized base-load mode during the period (0 h – 500 h)
ii. Grid frequency stability mode during the period (500 h – 505 h)
iii. Full power base-load mode during the period (505 h – 1500 h)

The representative power pattern under the described modes of reactor operation patterns is shown in Fig. 5. The power pattern is induced by considering the varying grid demands to fulfill the energy requirements. The variation in neutron flux corresponding to various operating modes effects the activation of CPs. If the reactor operates at a specific power level, the flux also maintains its constant value. However, adjustment in the reactor operating power directly affect the neutron flux, it increases with an increase in power level and vice versa. The CPA-AP1000 code was employed

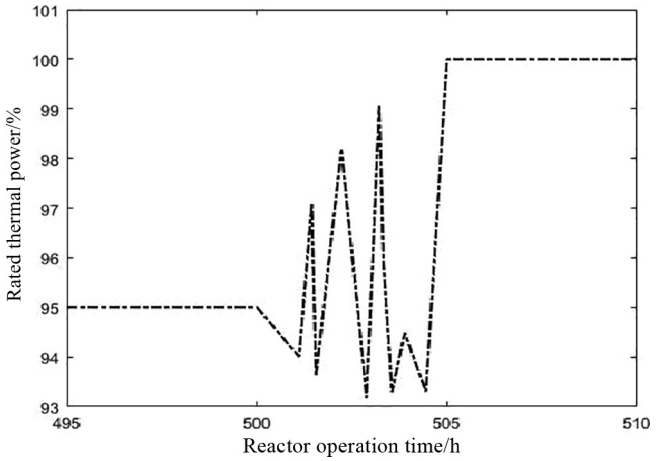

Fig. 5. Typical power fluctuations induced by the grid load variations.

Table 3
Fractional exchange rates of a typical PWR (Mirza et al., 2003).

Rate Description	Value1 and Unit	Value2 and Unit
Deposition on core	$\varepsilon_c Q_c/V_w = 5.835x10^{-5}s^{-1}$	$\varepsilon_c Q_c/V_c = 8.81x10^{-6}s^{-1}$
Deposition on piping	$\varepsilon_p Q_p/V_w = 1.00x10^{-6}s^{-1}$	$\varepsilon_p Q_p/V_c = 1.00x10^{-5}s^{-1}$
Ion-exchanger removal	$\varepsilon_I Q_I/V_w = 5.70x10^{-5}s^{-1}$	
Re-solution ratio for core	$K_c/V_w = 2.918x10^{-6}s^{-1}$	$K_c/V_c = 4.406x10^{-6}s^{-1}$
Re-solution ratio for piping	$K_p/V_w = 5.0x10^{-7}s^{-1}$	$K_p/V_p = 5.0x10^{-6}s^{-1}$
Volume of primary coolant	$V_w = 1.37x10^7 cm^3$	
Volume of scale on core	$V_c = 9.08x10^6 cm^3$	
Corrosion surface area	$S=1.01x10^8 cm^2$	
Average corrosion rate	$C_0 = 2.40x10^{-13} g \cdot cm^{-2} \cdot s^{-1}$	

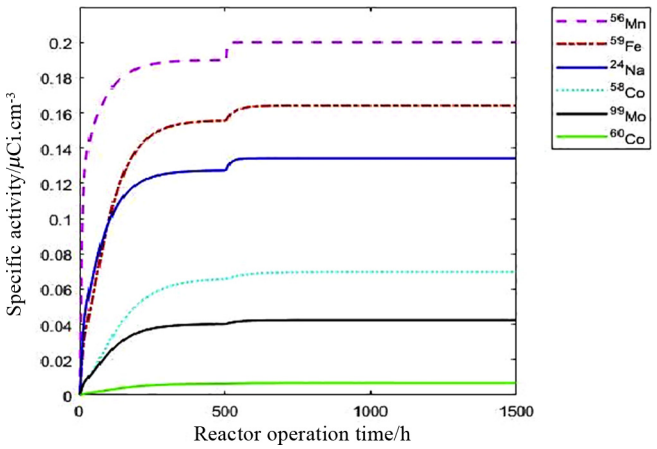

Fig. 6. The behavior of ACPs in primary coolant under various operating modes.

to study the behavior of dominant ACPs (^{56}Mn, ^{59}Fe, ^{24}Na, ^{60}Co and ^{99}Mo) in the primary circuit of AP-1000 during these specific operating modes. The results computed by CPA-AP1000 in above described operating modes are discussed in subsequent sections.

6.1.1. The behavior of ACPs in primary coolant under customized base-load mode

The reactor was operated under customized base-load mode at 95% RTP up to 500 h, and behavior of ACPs in primary coolant was simulated using CPA-AP1000. The response curves of ACPs during reactor operation in customized base-load mode have shown rapid growth in activity concentration at the beginning as presented in Fig. 6. The initial rapid increase in specific activity is due to higher corrosion rates during the early period of the reactor operation. This results in a rapid production of target materials at the beginning and ultimately production of more ACPs. After passing some time, CPs start accumulating on the inner surfaces coolant channel piping walls and on the core structures. Furthermore, CPs are also removed due to continuous ion exchange operation and the use of filters. A balance between the removal rate and accumulation of the CPs on piping and cores surfaces leads to a saturation specific activity value after passing sometime. So, corresponding ACPs have demonstrated constant values of specific activity after several hours of reactor operation in base-load mode.

6.1.2. The behavior of ACPs in primary coolant under grid frequency stability mode

The reactor was allowed to follow frequent power fluctuations within design limits during the period (500 h - 505 h). The specific activity caused by all of ACPs is noticed to be changed with the reactor power level fluctuations. The specific activity for all ACPs has shown a rapid rise and fall in value during the power fluctuations as shown in Fig. 7. The variation in specific activity behavior of corresponding ACPs under frequency fluctuation mode is governed by the rise and fall of operating power level. The variation in specific activity of ACPs under power fluctuations, is noticed to be strongly subjected to the pre-fluctuation specific activity values. The pre-fluctuation specific activity is a preparatory point for successive variation in specific activity during the power fluctuations. The behavior of ACPs after termination of power fluctuations was also studied. The post-fluctuation activity trend for all of ACPs is noticed to be intensely dependent on the level of final fluctuated power level, before the operating level switches to be stable. The activity of all of ACPs has demonstrated an increasing trend when the reactor was operated at a higher power level at the end of frequency stability mode. This shows that post-fluctuation specific activity is also a function of post-fluctuation operation power of the reactor.

6.1.3. The behavior of ACPs in primary coolant under full power base-load mode

The reactor was operated in full power base-load mode during the period (505 h – 1500 h) and simulation results of the corresponding ACPs are shown in Fig. 6. The results demonstrated that the corresponding ACPs raised slowly and finally gained new satu-

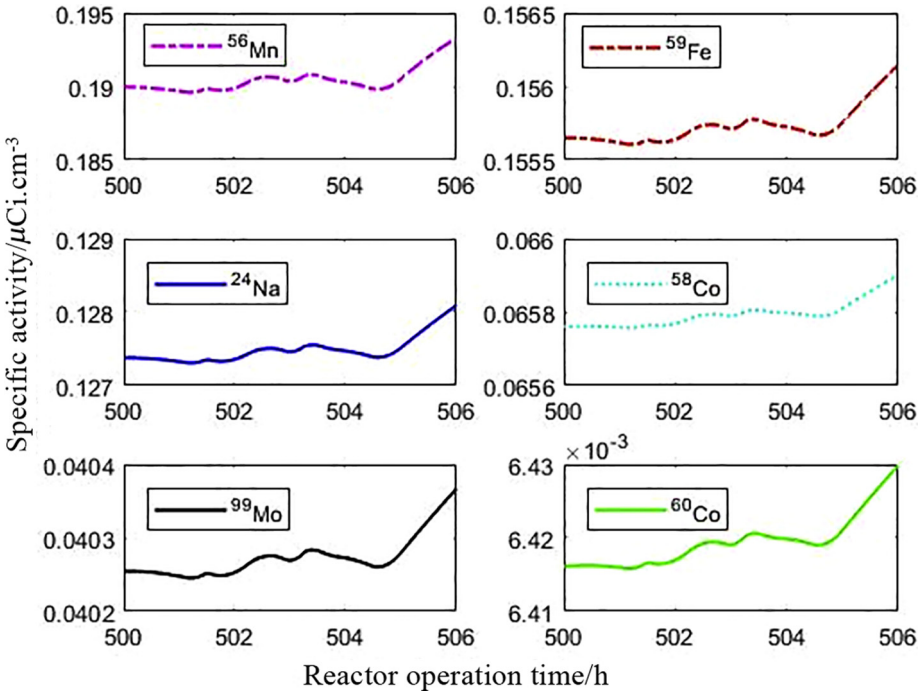

Fig. 7. The behavior of ACPs in primary coolant under frequency stability mode.

ration value when the reactor was operated at full power. The saturation value of corresponding ACPs under full power operation is noticed to be higher as compared to their values under customized base-load operation at 95% RTP. The results show that ^{56}Mn is the largest contributor to the total specific activity in primary coolant. It has a saturation value of 0.2000 μCi.cm^{-3} and contributes 32.40% to the total specific activity in primary coolant. The specific activity response of ^{56}Mn is rapid as compared to all of the other ACPs, it is mainly due to the short half-life as compared to other CPs of interest. The saturation specific activity of ^{59}Fe grows at a slower rate as compared to as that of ^{24}Na. However, the saturation specific activity of ^{59}Fe finally approaches a higher value of 0.1641 μCi.cm^{-3} as compared to 0.1342 μCi.cm^{-3} of ^{24}Na. The ^{59}Fe and ^{24}Na contribute 26.60% and 21.70% to the total specific activity respectively. The saturation activities of ^{58}Co, ^{99}Mo and ^{60}Co are 0.0698 μCi.cm^{-3}, 0.0425 μCi.cm^{-3} and 0.0068 μCi.cm^{-3} respectively. The ^{58}Co, ^{99}Mo and ^{60}Co contribute to the total specific activity of 11.30%, 6.89% and 1.11% respectively. These ACPs are noticed to contribute less towards the total specific activity during reactor operation. However, the activity caused by them retain for a longer period of time as compared to other ACPs, mainly because of their longer half-lives. The rounded off values of percentage contribution and saturation level of specific activity for different ACPs in the primary coolant are described in Fig. 8.

The saturation specific activity values of ACPs in AP-1000 and a reference PWR are compared under full power base-load mode as shown in Fig. 9. The saturation specific activity values of corresponding ACPs in AP-1000 and the reference PWR are in good agreement (Mahmood et al., 2018). The related difference in corresponding values is due to the difference of both reactor designs and dissimilar codes used for neutron flux calculations for AP-1000 and the reference PWR. The MCNP used for AP-1000 is the modern Monte Carlo based code and possess the ability to more accurately model the complex geometries. The MCNP has advantageously executed flux calculations for AP-1000 alone, as compared to the combination of codes LEOPARD and ODMUG used for the PWR for the same purpose. The neutronics calculations accomplished by MCNP are more reliable because it treats individual particles for neutronics calculations and uses updated built-in cross-section libraries. This showed that CPA-AP1000 is capable of calculating the behavior of ACPs with reasonable computational reliability.

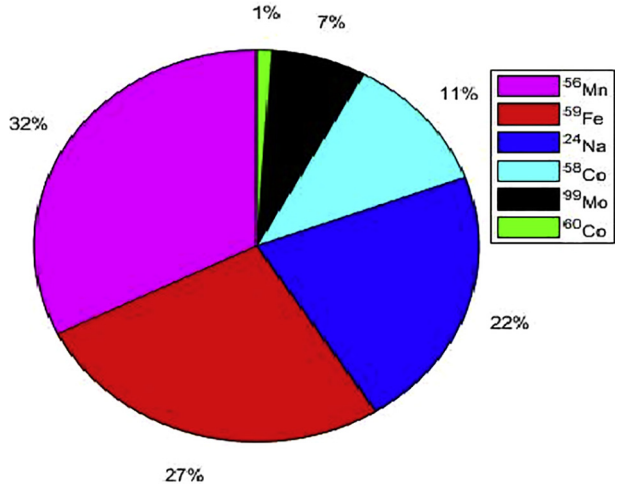

Fig. 8. Percentage contribution of different ACPs in primary coolant under normal full power operation.

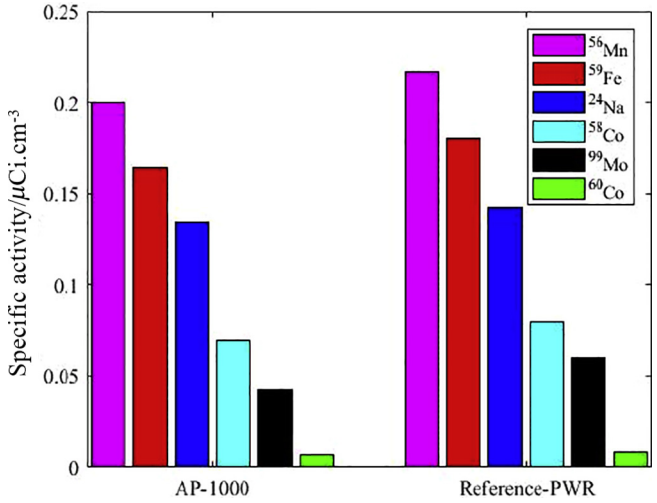

Fig. 9. Saturation specific activity of ACPs in primary coolant in AP-1000 and a reference PWR under full power base-load mode.

6.1.4. The behavior of ACPs in primary coolant and on inner walls

The investigations are further extended to compare the variation in behavior of ^{56}Mn, ^{58}Co, ^{24}Na and ^{60}Co in primary coolant and on inner walls of piping and core structure, under grid frequency stability mode. The simulation results for specific activity due to ^{56}Mn, ^{58}Co, ^{24}Na and ^{60}Co in various parts of coolant circuit under grid frequency stability mode are shown in Fig. 10.

The results depict that the core is the largest contributor to specific activity from ACPs (^{56}Mn, ^{24}Na, ^{58}Co, and ^{60}Co) followed by the coolant and pipes. The power fluctuations have pronounced and rapidly changing effect on specific activity in the primary coolant and on inner walls of structures inside the reactor core. However, this effect is noticed to be comparatively less prominent and slowly varying for inner walls of piping structures. This is due to the fact that dissolved and suspended CPs in the primary coolant are directly exposed to neutron flux while traversing through the reactor core during every pass. Similarly, the structures lying inside the reactor core are also directly and continuously exposed to the neutron flux. Nevertheless, the piping structure lying outside the reactor core is not directly and continuously exposed to the neutron flux. The primary coolant transports the ACPs through the pipes and they are progressively deposited on the inner walls of primary circuit piping. So, variation in specific activity on the walls of piping structures is less as compared to core and coolant. It is also noticeable that the specific activity due to ^{56}Mn and ^{24}Na swiftly changes in all parts of the circuit as the reactor power fluctuates. This effect is comparatively lethargic for ^{58}Co, ^{60}Co showing that the activity of ^{58}Co and ^{60}Co activity is less vulnerable to smaller and frequent power fluctuations. But, its activity retains for a longer period of time and causes a continuous source of activity and radiation dose. This is mainly due to the longer half-life of ^{58}Co, ^{60}Co as compared to ^{56}Mn and ^{24}Na. This infers that ACPs with shorter half-lives are more vulnerable to frequent changes in specific activity as compared to ACPs with a longer half-life. However, ACPs with longer half-lives are of more importance as the ORE caused by them retains for a longer period resulting in the substantial delay in operation and maintenance activities.

7. Conclusions

The fresh reactor designs are made mandatory to be capable of complying with grid frequency transients, contrary to earlier NPPs

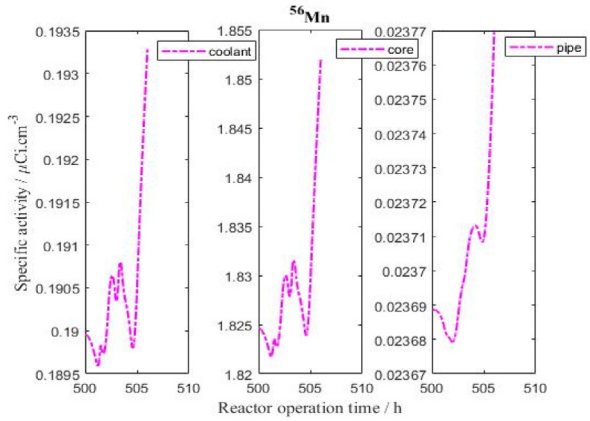

(a) ^{56}Mn behavior in various parts of the coolant circuit

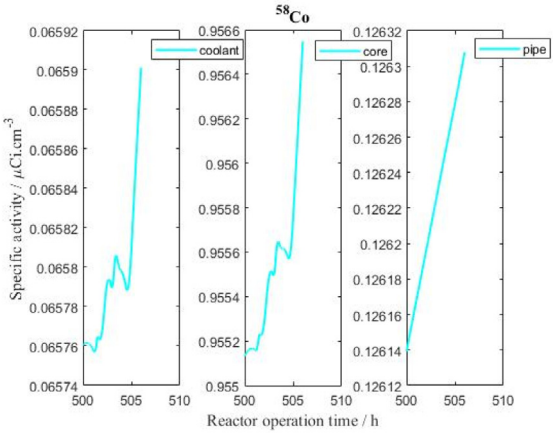

(c) ^{58}Co behavior in various parts of the coolant circuit

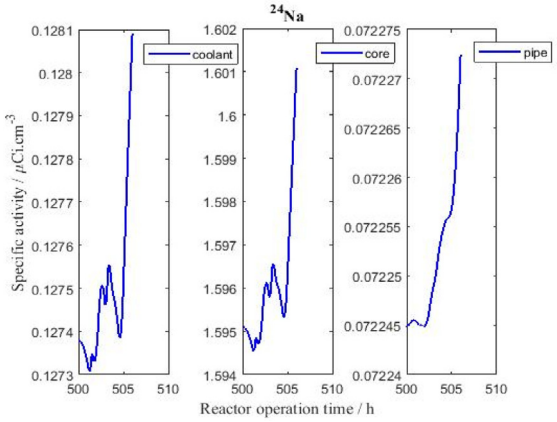

(b) ^{24}Na behavior in various parts of the coolant circuit

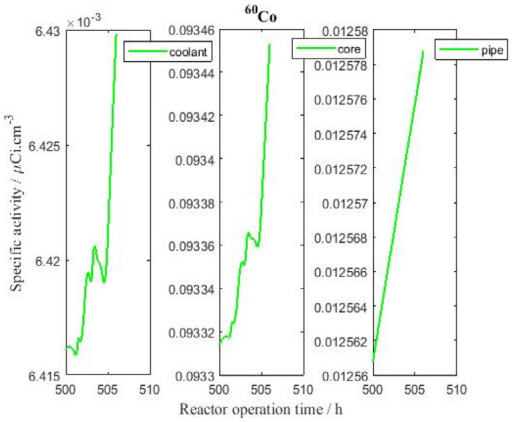

(d) ^{60}Co behavior in various parts of the coolant circuit

Fig. 10. Specific activity behavior of (a) ^{56}Mn, (b) ^{24}Na, (c) ^{58}Co and ^{60}Co in primary coolant and on inner walls of core and piping structure.

which have been typically operated in the base-load mode only. The AP-1000 has a strong capability to adopt the demand for participation in grid frequency control. On the other hand, it is vulnerable for frequent variations in the specific activity of the ACPs in the primary coolant circuit. The grid frequency stability mode causes rapid and frequent variations in the reactor operating power levels. An in-house developed code CPA-AP1000 is modified to accommodate such frequent power transients. A typical pattern of reactor operating power is induced during reactor operation, which includes customized base-load, frequency stability and full power base-load modes. The simulations are executed using modified CPA-AP1000 code to study the behavior of corresponding ACPs (^{56}Mn, ^{24}Na, ^{59}Fe, ^{58}Co, ^{99}Mo and ^{60}Co) in primary coolant for reactor operation in all of these modes. The computational reliability of the CPA-AP1000 was tested by comparing values of corresponding ACPs in AP-1000 and a reference PWR under the full power base-load mode. The values of ACPs in AP-1000 have demonstrated a good agreement with the corresponding values for a reference PWR. The results lead to infer that variation in coolant activity of corresponding ACPs under frequency stability mode is governed by the operating power fluctuations. The post-fluctuation specific activity of ACPs is also explored and found to directly follow the post-fluctuation operating power levels. It is noticed to be significantly dependent on the post-fluctuation operating power level as well.

The variation in behavior of ^{56}Mn, ^{24}Na, ^{58}Co and ^{60}Co in primary coolant and on inner walls of piping and core structure is also investigated under grid frequency stability mode. The corresponding ACPs are found in the highest concentration inside the core followed by the coolant and piping structure. The results show that ACPs with shorter half-lives are more vulnerable to frequent power changes as compared to those with longer half-lives. However, ACPs with longer half-lives are vital as they retain longer to cause dose for a longer period. They ultimately cause a substantial interruption in operation and maintenance schedules. The investigations provide a good insight of ACPs behavior in scenarios that can occur frequently during reactor operation. The study has presented a reasonable computational assessment of ACPs for a fresh reactor design complying with the modern grid environment. The results are helpful in the assessment of on-power accessibility of primary coolant circuit for operation and maintenance crews. The investigations have also drawn attention to conduct operational experiments for modern operating strategies recently introduced in AP-1000. The study can be extended to envisage the behavior of ACPs under more design-based operating scenarios.

Acknowledgment

The present work has been supported by the China Scholarship Council (CSC) Grant No. 2016GXZO22. The authors gratefully acknowledge the funding supports by China National Nuclear Corporation and Shanghai Nuclear Engineering Research & Design Institute, and as well as the fund of National Science and Technology Major Project, Grant No. MTR-ZB01K01W16-004. The authors

would like to thank their colleague Dr. Pengfei Wang for valuable insight and recommendations about AP-1000 core control strategies.

References

Chinese AP1000s pass commissioning milestones, 2018. World Nuclear News; Available from: http://www.world-nuclear-news.org/NN-Chinese-AP1000s-pass-commissioning-milestones-2206184.html.

Benfarah, M., Zouiter, M., Jobert, T., Dacquait, F., Bultot, M., Genin, J.-B., 2016. PWR circuit contamination assessment tool. Use of OSCAR code for engineering studies at EDF. EPJ Nucl. Sci. Technol. 2.

Deeba, F., Mirza, A.M., Mirza, N.M., 1999. Modeling and simulation of corrosion product activity in pressurized water reactors under power perturbations. Ann. Nucl. Energy 26, 561–578.

Drudy, K.J., Morita, T., Connelley, B.T., 2009. Robustness of the MSHIM Operation and Control Strategy in the AP1000 Design, 17th International Conference on Nuclear Engineering (ICONE17). Belgium, Brussels, pp. 893–904.

Guo, Q., Zhang, J., Fang, S., Chen, Y., 2018. Calculation and analysis of water activation products source term in AP1000. Prog. Nucl. Energy 109, 66–73.

IAEA, 2012. Modelling of Transport of Radioactive Substances in the Primary Circuit of Water-Cooled Reactors, IAEA-TECDOC-1672. Viana, Austria.

Jia, J., 2016. Research on Modeling the corrosion, activity and transport proceeds in PWR primary circuits School of Nuclear Science and Technology. Xi'an Jiaotong University, Xi'an, China.

Mahmood, F., Hu, H., Cao, L., 2018. Dynamic response analysis of corrosion products activity under steady state operation and Mechanical Shim based power-maneuvering transients in AP-1000. Ann. Nucl. Energy 115, 16–26.

Malik, J.I., Mirza, N.M., Mirza, S.M., 2012. Time-dependent corrosion product activity in a typical PWR due to changes in coolant chemistry for long-term fuel cycles. Prog. Nucl. Energy 58, 100–107.

Mirza, A.M., Mirza, N.M., Mir, I., 1998. Simulation of corrosion product activity in pressurized water reactors under flow rate transients. Ann. Nucl. Energy 25, 331–345.

Mirza, N.M., Rafique, M., Hyder, M.J., Mirza, S.M., 2003. Computer simulation of corrosion product activity in primary coolants of a typical PWR under flow rate transients and linearly accelerating corrosion. Ann. Nucl. Energy 30, 831–851.

Mirza, S.M., Rafique, M., Ahmad, F., Mirza, N.M., 2010. Static and dynamic sensitivity analysis of corrosion product activity in primary coolant circuits of pressurized water reactors. Prog. Nucl. Energy 52, 648–654.

Mo Shuran, J.J., Yichen, Bao, Xiuqiang, Shi, Wang Dongming, Xu., Xuelian, Xie Yongcheng, Huasi, Hu., 2016. Modeling of materials corrosion inside RCS based on mixed-conduction model, Proceedings of 8th International Symposium on Symbiotic Nuclear Power Systems for 21st Century September 26–28, 2016. Chengdu, China.

Nasir, R., Mirza, S.M., Mirza, N.M., 2017. Evaluation of Corrosion Product Activity in a Typical PWR with Extended Cycles and Flow Rate Perturbations. World J. Nucl. Sci. Technol. 07, 24–34.

NEA, 2011. Technical and Economic Aspects of Load Following with Nuclear Power Plants. Nuclear Energy Agency.

Ponciroli, R., Cammi, A., Lorenzi, S., Luzzi, L., 2015. Control approach to the load frequency regulation of a Generation IV Lead-cooled Fast Reactor. Energy Convers. Manage. 103, 43–56.

Rafique, M., Mirza, N., Mirza, S., J. Iqbal, M., 2010. Review of computer codes for modeling corrosion product transport and activity build-up in light water reactors.

Shim, H.-S., Park, M.-S., Baek, S.H., Hur, D.H., 2018. Effect of aluminum oxide coated on fuel cladding surface on crud deposition in simulated PWR primary water. Ann. Nucl. Energy 121, 607–614.

Snoj, L., Ravnik, M., 2006. Calculation of Power Density with MCNP in TRIGA Reactor, International Conference Nuclear Energy for New Europe, September 18–21, 2006. Portorož, Slovenia.

Stefani, G.L., Rossi, P.R., Maiorino, J.R., Santos, T.A., 2015. Neutronic and Thermal-Hydraulic Calculations for the AP-1000 NPP With the MCNP6 and Serpent Codes, 2015 International Nuclear Atlantic Conference - INAC, SP, Brazil.

Tang, Z., Wang, P., Fang, H., Li, C., Zhao, F., Hu, P., 2014. Development of a simulation platform for studying on primary frequency regulation characteristics of nuclear units. Prog. Nucl. Energy 70, 54–63.

Wang, P., Fu, Y., Wei, X., Zhao, F., 2018. Simulation study of frequency control characteristics of a generation III + nuclear power plant. Ann. Nucl. Energy 115, 502–522.

Westinghouse, 2005. AP1000 Design Control Document Rev. 15

Zhang, J., Li, L., He, S., Chen, Y., 2016. Calculation of Radioactivity and Dose Rate of Activated Corrosion Products in Water-Cooled Fusion Reactor. Sci. Technol. Nucl. Installations 2016, 1–6.